Structure
Article

Phosphorylation of DCC by ERK2 Is Facilitated by Direct Docking of the Receptor P1 Domain to the Kinase

Wenfu Ma,[1,2] Yuan Shang,[3] Zhiyi Wei,[3] Wenyu Wen,[1,2] Wenning Wang,[1,2,*] and Mingjie Zhang[1,2,3,*]
[1]Department of Chemistry
[2]Institute of Biomedical Sciences
Fudan University, Shanghai, P.R. China
[3]Division of Life Science, Molecular Neuroscience Center, State Key Laboratory of Molecular Neuroscience,
Hong Kong University of Science and Technology, Clearwater Bay, Kowloon, Hong Kong, P. R. China
*Correspondence: wnwang@fudan.edu.cn (W.W.), mzhang@ust.hk (M.Z.)
DOI 10.1016/j.str.2010.08.011

SUMMARY

Netrin receptor DCC plays critical roles in many cellular processes, including axonal outgrowth and migration, angiogenesis, and apoptosis, but the molecular basis of DCC-mediated signaling is largely unclear. ERK2, a member of the MAPK family, is one of the few proteins known to be involved in DCC-mediated signaling. Here, we report that ERK2 directly interacts with DCC, and the ERK2-binding region was mapped to the conserved intracellular P1 domain of the receptor. The structure of ERK2 in complex with the P1 domain of DCC reveals that DCC contains a MAPK docking motif. The docking of the P1 domain onto ERK2 physically positions several phosphorylation sites of DCC in the vicinity of the kinase active site. We further show that the docking interaction between the P1 domain and ERK2 is essential for the ERK2-mediated phosphorylation of DCC. We conclude that DCC signaling is directly coupled with MAPK signaling cascades.

INTRODUCTION

DCC (deleted in colorectal cancer), first isolated as a candidate tumor-suppressor gene due to its frequent deletions in colorectal cancers (Fearon et al., 1990), encodes a single transmembrane protein which has subsequently been shown to be a netrin receptor (Keino-Masu et al., 1996). The netrin/DCC signaling pathway mediates axon outgrowth and guidance (Fazeli et al., 1997; Keino-Masu et al., 1996; Kolodziej et al., 1996). DCC not only mediates netrin-induced axon attraction but also participates in repulsive axon guidance together with UNC5, another netrin receptor (Chan et al., 1996; Hong et al., 1999; Leonardo et al., 1997). DCC is a type I transmembrane protein that possesses immunoglobulin (Ig) repeats and fibronectin type III (FNIII) repeats in its extracellular region. Its cytoplasmic domain contains three conserved sequence motifs, named P1, P2, and P3 (Kolodziej et al., 1996), although no well-defined structural domains or catalytic activity have been identified thus far for the DCC cytoplasmic domain. Both in vitro and in vivo studies have demonstrated that the attractive response of DCC to netrins specifically originates from the cytoplasmic domain of the receptor, as a chimera DCC in which the extracellular portion of DCC is fused with the cytoplasmic part of UNC5 elicited repulsive responses to netrin (Hong et al., 1999; Keleman and Dickson, 2001). Due to the lack of catalytic motifs in its intracellular domain, DCC is thought to transmit its signal by binding to its downstream proteins. Identification of DCC intracellular domain binding partners has helped in understanding netrin/DCC downstream signaling events. For example, FAK and Src family kinase Fyn were identified to interact with the P3 domain of DCC, and netrin stimulation induced tyrosine phosphorylation of the receptor by both kinases (Li et al., 2004; Liu et al., 2004; Rajasekharan et al., 2009; Ren et al., 2004). The disruption of either FAK signaling or Src family kinase activity abolished netrin-induced axon outgrowth and attractive growth cone turning. Netrin stimulation of neurons has also been found to induce DCC-dependent MAP kinase activation, which is essential for neurite outgrowth and directed axon migrations (Campbell and Holt, 2003; Forcet et al., 2002). Other proteins found to be involved in netrin/DCC signaling include myosin X (Zhu et al., 2007), Dock180 (Li et al., 2008), and PITPα (Xie et al., 2005). Interestingly, essentially all known DCC-binding proteins bind to the conserved P3 domain of DCC. It is worth noting that functional studies have demonstrated that the conserved P1 and P2 domains are required for the axonal guidance activity of DCC (Hong et al., 1999; Keleman and Dickson, 2001). Therefore, it is predicted that there remain unidentified proteins capable of interacting with the P1 and/or P2 regions of DCC.

Both DCC and UNC5 have also been shown to be intimately linked to cell survival. It has been proposed that both DCC and UNC5 function as dependence receptors for netrins. The engagement of DCC and UNC5 with netrins promotes cell survival, whereas the absence of netrins stimulates cell death (Goldschneider and Mehlen, 2010; Llambi et al., 2001). The downregulation of DCC and/or the upregulation of netrins promotes cell survival and tumor formation (Arakawa, 2004; Fitamant et al., 2008; Mazelin et al., 2004; Thiebault et al., 2003).

MAP kinases are evolutionarily conserved enzymes linking cell surface receptors to intracellular regulatory targets. In the MAPK

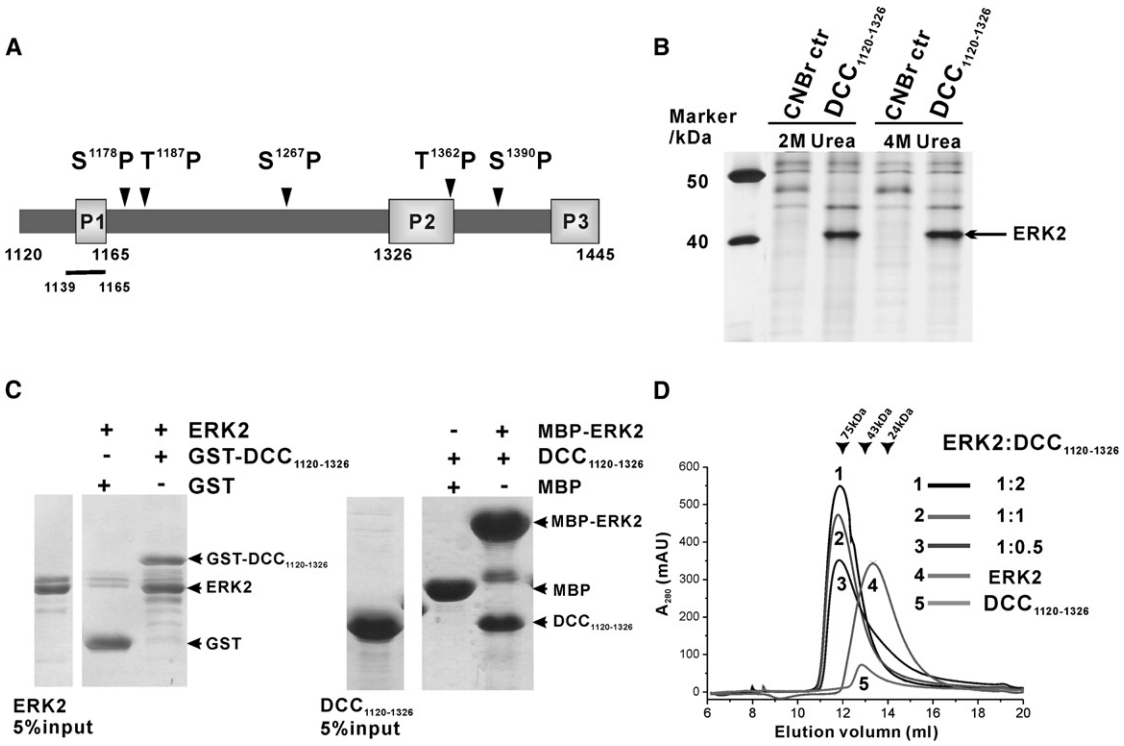

Figure 1. Direct Interaction of DCC with ERK2

(A) Schematic diagram of the cytoplasmic domain organization of DCC. The short bar denotes the synthetic docking peptide to ERK2. The figure also shows five potential ERK2 phosphorylation sites of DCC.

(B) Affinity chromatographic purification of proteins that associate with the $DCC_{1120-1326}$ fragment from rat brain lysate. "CNBr ctr" stands for the control purification using the CNBr-activated Sepharose beads without coupling of the $DCC_{1120-1326}$ fragment. The figure shows the silver staining of the proteins eluted with a buffer containing 2 and 4 M urea, respectively. The mass spectroscopy analysis of the phosphorylation state of the pulled down ERK2 is shown in Figure S1.

(C) Pull-down experiments showing the direct interaction between DCC and ERK2. In the left panel, GST-tagged $DCC_{1120-1326}$ was used to pull-down untagged ERK2. In the right panel, MBP-tagged ERK2 was used to pull down untagged $DCC_{1120-1326}$.

(D) Analytical gel-filtration chromatography showing that $DCC_{1120-1326}$ binds to ERK2 with 1:1 stoichiometry (see also Figure S1).

signaling pathway, three conserved kinases (MAPKKKK, MAPKK, MAPK) are activated in series by extracellular stimuli and regulate key cellular functions, including proliferation, differentiation, migration, and apoptosis, and participate in a number of disease states, including chronic inflammation and cancer (Park et al., 2007). For example, the ERK1/2 (extracellular signal-regulated 1/2)-MAP kinase pathway is well known to be linked to a large percentage of human cancers, and tumorigenesis is typically associated with the activation of the ERK signaling pathways (Downward, 2003; Hoshino et al., 1999). Interestingly, the netrin/DCC-mediated axonal migration is known to be linked to ERK1/2 activation (Campbell and Holt, 2003; Forcet et al., 2002), although the exact molecular basis of the DCC-ERK1/2 connection is unclear. Nonetheless, the functional connection of DCC and ERK1/2 fits well with the dependence-receptor hypothesis of DCC.

Here, we report that DCC interacts directly with ERK2 through its intracellular P1 domain. The crystal structure of inactive ERK2 in complex with a DCC peptide reveals a docking motif-mediated binding of DCC to ERK2. We discover that DCC is a direct substrate of ERK2. We also show that the docking interaction is required for the phosphorylation of DCC by ERK2. Our findings indicate that netrin/DCC-induced activation of ERK2 can directly regulate cellular signaling events of DCC via its phosphorylation.

RESULTS

DCC Directly Interacts with ERK2

As the first step in understanding DCC-mediated signaling events, we attempted to identify DCC-interacting proteins from rat brains using affinity chromatography with various purified intracellular DCC fragments as the bait. Purified proteins were subjected to mass spectrometry analysis for identification. Such affinity-based purification using the bait $DCC_{1120-1326}$, which includes the juxtamembrane region and the conserved P1 domain of DCC (Figure 1A), identified ERK2 as a prominent DCC binder (Figure 1B). Mass spectroscopy analysis showed that the pulled down ERK2 is unphosphorylated (see Figure S1 available online). Importantly, ERK2 was not detected in parallel affinity purifications using DCC-P2&3 (1327–1445) and DCC-P3 (1374–1445) as baits (data not shown), indicating that the association of DCC with ERK2 is specifically mediated by the N-terminal part of the DCC intracellular domain. We then examined the potential direct interaction between $DCC_{1120-1326}$ and ERK2 using in vitro pull-down assays. Purified

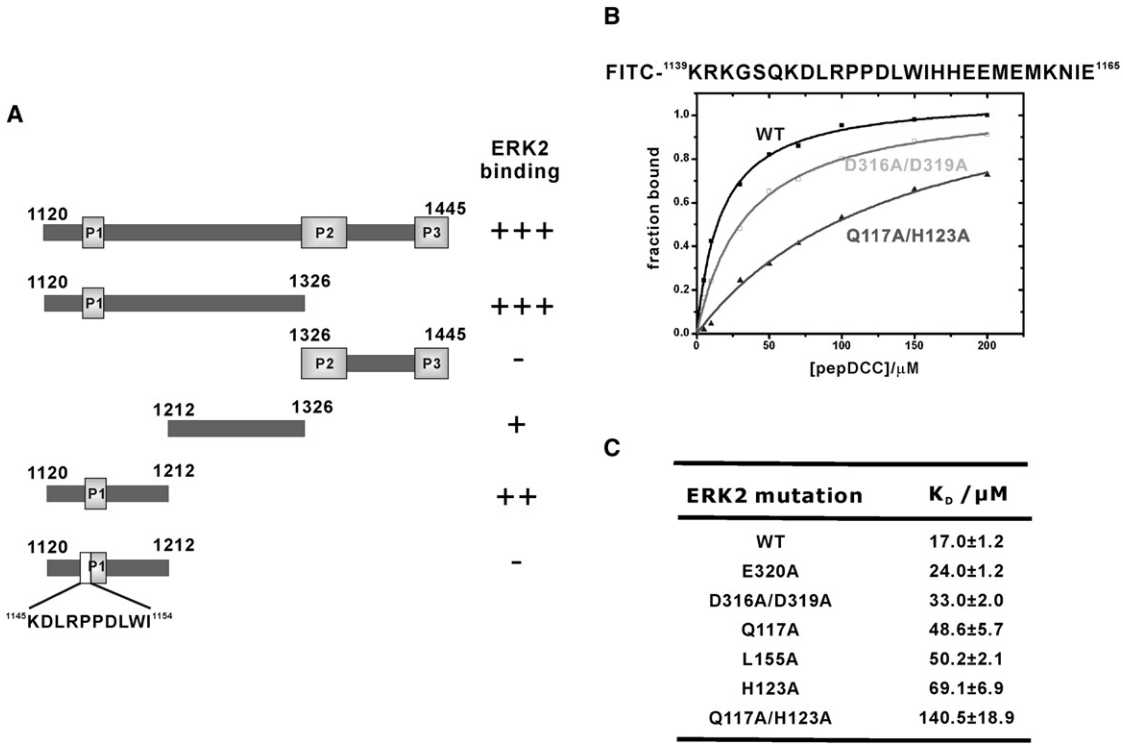

ERK2 mutation	K_D / μM
WT	17.0±1.2
E320A	24.0±1.2
D316A/D319A	33.0±2.0
Q117A	48.6±5.7
L155A	50.2±2.1
H123A	69.1±6.9
Q117A/H123A	140.5±18.9

Figure 2. Characterization of the Interaction between DCC and ERK2

(A) Summary diagram showing the mapping of the ERK2 binding site on DCC. The data were derived from the pull-down and analytical gel-filtration assays shown in Figures 1C and 1D. The qualitative bind strengths of various DCC fragments to ERK2 are categorized as strong ("+++"), medium ("++"), weak ("+"), and non-detectable ("−"). The open square indicates the deletion of 10 residue (1145–1154) from DCC that eliminated the ERK2/DCC interaction.

(B) Fluorescence polarization-based measurement of the binding affinities of the WT and various point mutations of ERK2 with the FITC-labeled DCC peptide. For clarity, only representative binding curves are shown in the figure.

(C) K_D values of the bindings of ERK2 and its mutants with the DCC peptide derived from the fluorescence experiment (see also Figure S2).

GST-$DCC_{1120\text{-}1326}$ robustly pulled down untagged ERK2 (Figure 1C). Reciprocally, MBP-tagged ERK2 was shown to interact with untagged $DCC_{1120\text{-}1326}$ (Figure 1C). The specific interaction between ERK2 and $DCC_{1120\text{-}1326}$ was further verified using analytical gel-filtration chromatography (Figure 1D). The gel-filtration experiment indicates that ERK2 and $DCC_{1120\text{-}1326}$ can form a 1:1 complex with a molecular mass of ~75 kDa (Figure 1D).

The P1 Domain of DCC Is Responsible for Binding to ERK2

We next tried to map out the minimal ERK2 binding region of DCC using the pull-down assay shown in Figure 1C. The entire cytoplasmic tail of DCC, containing the P2 and P3 regions in addition to the $DCC_{1120\text{-}1326}$, displayed no observable differences from the $DCC_{1120\text{-}1326}$ fragment in binding to ERK2. Consistent with this observation, the DCC fragment containing the P2 and P3 fragments only showed no detectable binding to ERK2 (Figure 2A). We further divided $DCC_{1120\text{-}1326}$ into two fragments. The N-terminal fragment (residues 1120–1212) contains the highly conserved P1 domain, while the sequence of the C-terminal fragment (1212–1326) is less conserved. The pull-down-based assay showed that the $DCC_{1120\text{-}1212}$ fragment displays prominent binding to ERK2, although the binding is slightly weaker than that of the $DCC_{1120\text{-}1326}$ fragment (Figure 2A). Interestingly, the $DCC_{1212\text{-}1326}$ fragment also showed weak but consistently detectable binding to ERK2 (Figure 2A). Thus, we conclude that the cytoplasmic tail of DCC contains two ERK2 binding sites, with the $DCC_{1120\text{-}1212}$ fragment being the stronger site and the $DCC_{1120\text{-}1326}$ fragment the weaker site. The 1:1 stoichiometry of the ERK2/DCC complex shown in the gel filtration column implies that the two binding sites of one DCC molecule synergistically interact with one ERK2, explaining the strong interaction between DCC and ERK2 observed in the affinity-based purification and the in vitro pull-down assay shown in Figure 1.

We quantified the binding affinity of the $DCC_{1120\text{-}1212}$/ERK2 complex using ITC titration and obtained a K_d of 20.0 μM (Figure S2). The highly conserved P1 domain has previously been identified to be required for DCC to function properly (Hong et al., 1999). We reasoned that the P1 domain might be required for DCC to bind to ERK2. Indeed, the deletion of a 10 residue peptide fragment containing the first six amino acids of P1 domain plus the four amino acids preceding the P1 domain (^{1145}KDLRPPDLWI^{1154}) completely abolished the binding of $DCC_{1120\text{-}1212}$ to ERK2 (Figure 2A). We further discovered that a 27 residue synthetic peptide containing the P1 domain of DCC (^{1139}KRKGSQKDLRPPDLWIHHEEMEMKNIE^{1165}, referred to as the DCC peptide) displayed an ERK2 binding affinity equal to that of the $DCC_{1120\text{-}1212}$ fragment (K_d ~17.0 μM)

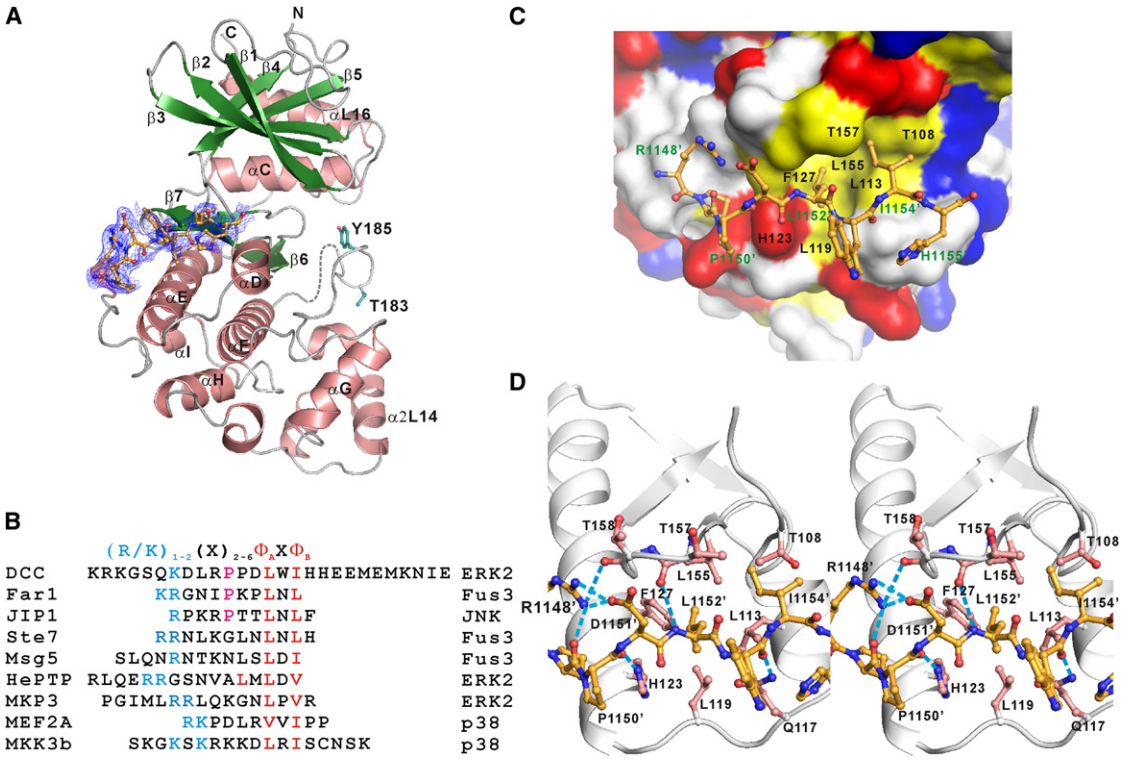

Figure 3. The Crystal Structure of the ERK2/DCC Peptide Complex

(A) Ribbon diagram of the ERK2/DCC peptide complex. The disordered region is shown in dotted line. The DCC peptide is shown in a stick-and-ball model. The omit map calculated with a model without DCC peptide is contoured at 1.0 σ. The two phosphorylation sites (Thr183 and Tyr185) in the activation loop of ERK2 are also shown in the stick model.

(B) Sequence alignment of the DCC peptide with the selected MAPK docking motif peptides. The hydrophobic residues in the ØA and ØB positions and the basic residues upstream of the "ØA-X-ØB"-motif are highlighted in red and blue, respectively. The protein names at the left are from which each docking sequence resides, and the kinase names at the right stand for the MAPK to which each docking sequence binds.

(C) Surface representation of ERK2 in complex with the DCC peptide (in the stick model). The hydrophobic, positively charged, negatively charged and uncharged polar residues are colored in yellow, blue, red, and white, respectively.

(D) Stereoview of the detailed interactions between the DCC peptide (golden) and the docking groove of ERK2 (pink). Dotted lines denote hydrogen bonds and salt bridges.

(Figure 2B; Figure S1), indicating that this 27 residue synthetic peptide contains all necessary elements (with respect to the $DCC_{1120-1212}$ fragment) for binding to ERK2.

Structure of the ERK2/pepDCC Complex

To elucidate the molecular basis of the DCC-ERK2 interaction, we determined the crystal structure of catalytically inactive ERK2 in complex with the DCC peptide at a resolution of 1.95 Å. The structure of the ERK2/DCC peptide complex was solved by molecular replacement using the inactive ERK2 structure (PDB code 1ERK) as the search model. Except for the few residues in the activation loop (residues 174–178 and Lys201) and several residues at the two termini, the entire length of ERK2 was well resolved in the refined model of the ERK2/DCC peptide complex (Figure 3A). Compared to ERK2, the electron densities of the residues from the DCC peptide were relatively weak. Nevertheless, we were able to clearly trace the electron densities of the eight residues in the middle of the peptide (^{1148}RPPDLWIH^{1155}) (Figure 3A), and this stretch of the DCC peptide was shown to be essential for binding to ERK2 in Figure 2A.

The structure of the ERK2/DCC peptide complex clearly shows that the DCC peptide binds to the so-called "docking motif-binding site" of ERK2 (Figure 3A), a mode conserved in MAP kinases when binding to their substrates/regulatory enzymes (Carvalho et al., 2006; Zhou et al., 2006). Amino acid sequence analysis of the DCC peptide with the known MAPK "docking motifs" indeed reveals that the DCC peptide (^{1148}RPPDLWI^{1154}) contains the signature "$(K/R)_{1-2}$-X_{2-6}-$Ø_A$-X-$Ø_B$" sequence found in all MAPK "docking motifs" (Figure B), explaining the specific binding between DCC and ERK2 as well as hinting at DCC as a potential direct substrate of ERK2. In the ERK2/pepDCC complex, the DCC peptide adopts an extended conformation and binds to the hydrophobic docking groove of ERK2 (Figure 3C). Intramolecular interactions, including a hydrogen bond between Arg1148′Nη (prime denotes the residues from the DCC peptide) and the carbonyl oxygen of Pro1149′ and a bidentate salt bridge between Arg1148′ and Asp1151′, stabilize the poly-proline helix II conformation of the ^{1148}RPPD^{1151} segment of the DCC peptide and facilitate the formation of two pairs of inter-DCC/ERK2 hydrogen bonds (between the carbonyl of Pro1150′ and the Nε of His123 side

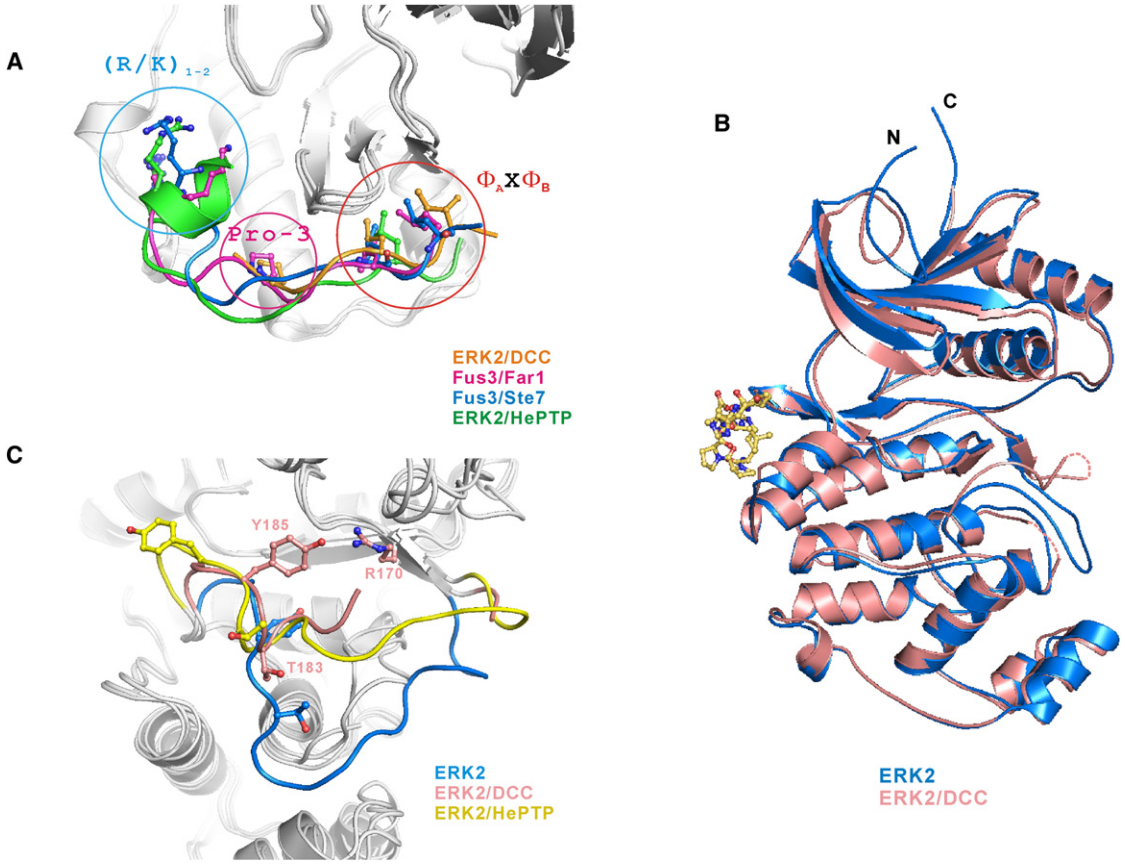

Figure 4. DCC Binding-Induced Conformational Changes of ERK2

(A) Comparison of the conformations of the different docking peptides in structures of the ERK2/DCC, Fus3/Far1, Fus3/Ste7, and ERK2/HePTP complexes. The ØA and ØB and R/K residues are shown in the stick model.

(B) Superposition of the backbone structures of the inactive ERK2 and ERK2 in the ERK2/DCC peptide complex showing the overall structural similarity of the two forms of ERK2 except for its activation loop.

(C) Superposition of the ERK2 structures in the inactive ERK2 (blue), the ERK2/DCC complex (pink), and the ERK2/HePTP complex (yellow) showing the conformational changes of the activation loop ERK2 upon binding to its docking peptides.

chain and between the carbonyl of T158 and Arg1148′Nη; Figure 3D). The formation of the poly-proline helix II conformation of the ^{1148}RPPD^{1151} segment also physically positions the hydrophobic side chain Pro1149′ (the Pro residue 3 residues upstream of $Ø_A$) into the edge of the hydrophobic pocket accommodating the $Ø_A$-X-$Ø_B$-motif (see below). The interaction between the $Ø_A$-X-$Ø_B$ sequence of DCC (^{1152}LWI^{1154}) and ERK2 is highly similar to those observed in MAP kinases in complex with their respective docking motifs (Carvalho et al., 2006; Zhou et al., 2006). The side chain of Leu1152′ ($Ø_A$ in the $Ø_A$-X-$Ø_B$ sequence) makes van der Waals contact with Leu113 in αD, Leu119 in αD-αE loop, Phe127 in αE, and Leu155 in β7 of ERK2. Ile1154′ ($Ø_B$) interacts with the side chains of Thr108 in αD, Leu155 in β7, and Thr157 in β7-β8 loop (Figure 3D). Two additional hydrogen bonds are formed between DCC and ERK2 (between backbone carbonyl oxygens Trp1153′ and Gln117Nε and between the backbone amide of Leu1152′ with the backbone carbonyl of Thr157) (Figure 3D).

Structure-based sequence alignment analysis of the MAP kinase docking peptides reveals that the DCC peptide most resembles the Fus3 substrate Far1 peptide and the JNK inhibitor JIP1 peptide, each sharing a conserved Pro 3 residues upstream of the $Ø_A$-X-$Ø_B$-motifs (Figure 3B). This Pro residue in the Far1 peptide was considered responsible for the unique conformation of the peptide, with respect to other peptides, in the structures of the Fus3/peptide complexes (Remenyi et al., 2005). Comparison of complex structures also showed that the conformation of the DCC peptide is most similar to those of the Far1 and JIP1 peptides in their respective kinase complex structures, with the Pro at $Ø_A$-3 occupying the same position on the MAPKs (Figure 4A).

The positively charged residue(s) in the (R/K)$_{1-2}$-(X)$_{2-6}$-$Ø_A$-X-$Ø_B$ docking motifs have been shown to be important for their binding to some MAP kinases, including ERK2 (Chang et al., 2002; Goldsmith et al., 2004). The DCC peptide also contains an Arg and a Lys at the $Ø_A$-4 and $Ø_A$-6 positions, respectively (Figure 3B). No direct charge-charge interactions occur between these two residues from DCC and the negatively charged residues in the CD site of ERK2 (Figure 4A). The formation of intramolecular salt bridges between Arg1148′ and Asp1151′ restrain the side chain of Arg1148′ from extending toward the ERK2 CD site. The electron density of Lys1151′ is completely invisible, suggesting that the interaction between this DCC Lys and the ERK2 CD

site is also minimal. It has been shown that the basic residues of the MEF2A/MKK3b peptides in complex with p38α are also highly disordered (Park et al., 2007). We directly tested the contributions of the potential charge-charge interaction between the positively charged residues of the DCC peptide and the negatively charged residues (Asp316, 319, and Glu320) in the CD site of ERK2 by substituting Asp316&319 or Glu320 with Ala. Consistent with the structural analysis, the single or double substitution mutation of ERK2 only showed marginal decreases in binding to the DCC peptide (Figures 2B and 2C). In contrast, mutations of the residues at the $Ø_A$-X-$Ø_B$-docking groove of ERK2 (Q117A, L155A, H123A, and Q117A/H123A substitutions) caused more evident decreases in binding to the DCC peptide (Figure 2C). These observations are consistent with the structural analysis of the complex, indicating that the hydrophobic and hydrogen bond interactions at the docking groove are essential for binding while the CD site interaction is less important.

Peptide Binding-Induced Conformational Changes in the ERK2 Activation Loop

The previous structural studies of MAP kinases revealed that docking motif peptide binding can induce local as well as long-range conformational changes (Zhou et al., 2006). Similar to the ERK2/HePTP complex, the overall structure of ERK2 in the ERK2/DCC peptide complex resembles active ERK2 more than inactive ERK2. Superimposing the complex structure with inactive (Zhang et al., 1994) and active ERK2 (Canagarajah et al., 1997) structures gives backbone root mean square deviations (rmsd) of 2.0 and 1.6 Å, respectively. The backbone rmsd between the two ERK2 structures in the ERK2/DCC and ERK2/HePTP complexes is 1.4 Å, indicating high structural similarity between the two ERK2 complexes. The binding of the DCC peptide does not induce substantial conformational changes in ERK2 except in the activation loop of the enzyme (Figure 4B). Prior to the determination of the ERK2/DCC complex structure, the activation loop of ERK2 was shown to adopt three distinct conformations, corresponding to the inactive, active, and docking peptide-bound forms of the enzyme (Akella et al., 2008; Zhou et al., 2006). In our structure, the conformation of the activation loop is most similar to that of the ERK2/HePTP complex, but also shows obvious differences (Figure 4C). As observed in the ERK2/HePTP complex, the binding of the DCC peptide exposes the dual phosphorylation sites in the activation loop (Thr183 and Tyr185) from the buried state in the inactive enzyme to the fully exposed state (Figure 4C). However, the side-chain orientations of Thr183 and Tyr185 are quite different in the two complex structures. Specifically, Tyr185 in ERK2/DCC forms a hydrogen bond with the side chain of Arg170, a residue that interacts with pT183 in active ERK2. Tyr185 in ERK2/HePTP points in the opposite direction (Figure 4C). The side-chain orientations of Tyr185 in both complexes significantly deviate from that in active ERK2. These observations suggest that the activation loop is intrinsically dynamic and subtly regulated both by docking interactions and by phosphorylations.

ERK2 Directly Phosphorylates DCC

Given that DCC contains several ERK2 phosphorylation motifs downstream of its kinase docking sequence (Figure 1A), we hypothesized that DCC is likely to be a substrate of the kinase. We tested this hypothesis by in vitro DCC phosphorylation assay. There are five potential phosphorylation sites in the cytoplasmic domain of DCC (aa 1120–1445), three within the $DCC_{1120\text{-}1326}$ fragment and the other two in the P2 domain and the P2/P3-linker region (Figure 1A). To map the individual ERK2 phosphorylation sites on DCC, we generated three DCC fragments with increasing lengths ($DCC_{1120\text{-}1212}$, $DCC_{1120\text{-}1326}$, and $DCC_{1120\text{-}1445}$), and performed time-dependent in vitro phosphorylation assays using MEK1-activated ERK2. ERK2-mediated phosphorylation of DCC fragments can be conveniently monitored by phosphorylation-induced mobility shifts of DCC bands on SDS-PAGE (Figure 5). The $DCC_{1120\text{-}1212}$ fragment contains two potential ERK2-phosphorylation sites (Ser1178 and Thr1187). Incubation of the $DCC_{1120\text{-}1212}$ fragment with active ERK2 resulted in two additional discrete bands of DCC with slower mobility, with the upper band being phosphorylated somewhat faster than the lower band, indicating that both Ser1178 and Thr1187 are phosphorylated by ERK2 (Figure 5A). Substitution of Ser1178 with Ala specifically eliminated the upper phosphor-DCC band (Figure 5A, middle panel), and substitution of both Ser1178 and Thr1187 with Ala completely abolished DCC phosphorylation by ERK2. The data in Figure 5A also indicate that the lower band represents the pT1187 form of the DCC fragment and the upper band stands for the pS1178 (or the pS1178/pT1187, thus the assignment of the phosphorylation state should be considered tentative) DCC. The phosphorylation of S1178 was also confirmed by mass spectroscopy identification (Figure S3). To determine whether S1267 might also be phosphorylated by ERK2, we tested the $DCC_{1120\text{-}1326}$ fragment. As expected, the WT $DCC_{1120\text{-}1326}$ can be efficiently phosphorylated by ERK2 (Figure 5B, middle). Clear phosphorylation of the $DCC_{1120\text{-}1326}$ fragment with both Ser1178 and Thr1187 substituted with Ala was observed (Figure 5B, left), indicating that Ser1267 can also be phosphorylated by ERK2, albeit more slowly. Consistent with this observation, the triple mutation (S1178A/T1187A/S1267A) completely eliminated $DCC_{1120\text{-}1326}$ phosphorylation by ERK2 (Figure 5B, right). We then used the whole cytoplasmic domain of DCC to identify whether the last two sites can be phosphorylated by ERK2. Again, the WT $DCC_{1120\text{-}1445}$ shows clear phosphorylation-induced mobility shifts. In contrast, the S1178A/T1187A/S1267A mutant of $DCC_{1120\text{-}1445}$ showed no detectable mobility shift after prolonged incubation with active ERK2 (Figure 5C). Therefore, we conclude that the last two predicted ERK2 phosphorylation sites (Thr1362 and Ser1390) are not phosphorylated by ERK2, and that all the ERK2 phosphorylation sites on DCC are located within the linker between P1 and P2.

Finally, we tested the role that the ERK2 docking sequence of DCC plays in its phosphorylation by the kinase. We generated a deletion mutant of DCC ($DCC_{1120\text{-}1326}$Δ1145-1154), and the mutant DCC was defective in binding to ERK2 (data not shown). As shown in Figure 5D, $DCC_{1120\text{-}1326}$Δ1145-1154 showed no detectable phosphorylation by ERK2 even after incubation for 7 hr with the active kinase, indicating that the docking of DCC to ERK2 is required for its phosphorylation by the kinase.

DISCUSSION

In this work, we confirm that DCC directly interacts with ERK2, supporting the hypothesis that the netrin/DCC complex signaling

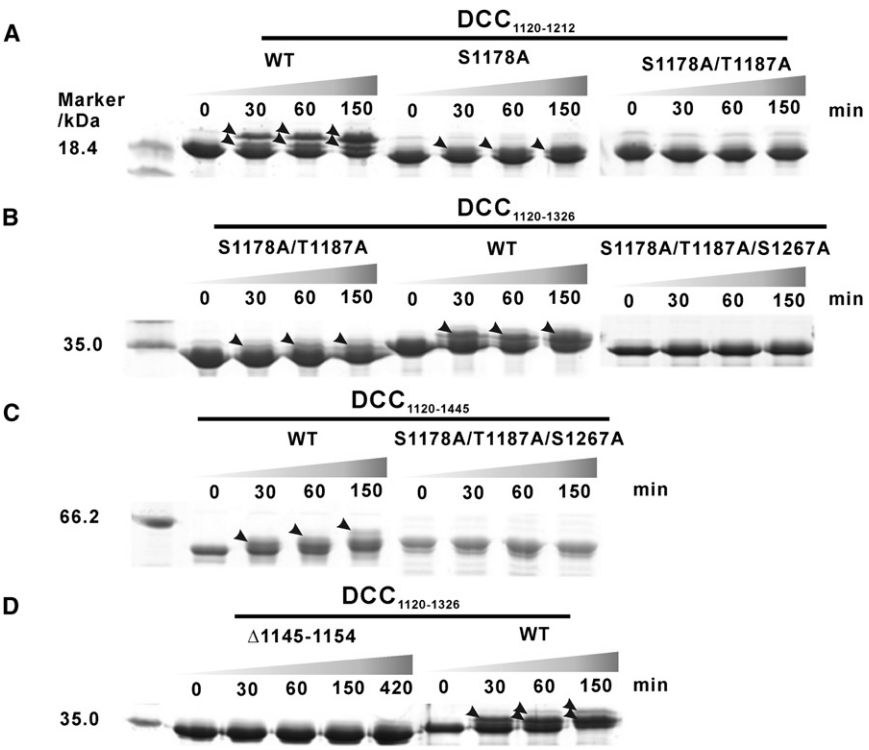

Figure 5. ERK2 Directly Phosphorylates DCC

(A) The $DCC_{1120-1212}$ fragment phosphorylation by ERK2 assayed by the time-dependent, phosphorylation-induced mobility shift of the DCC fragments. The WT $DCC_{1120-1212}$ displays two additional bands with slower mobility after phosphorylation (indicated by arrow heads, left). The substitution of Ser1178 with Ala eliminated the top band observed in the WT protein (middle). Mutation of both Ser1178 and Thr1187 completely eliminated the phosphorylation-induced mobility shift of $DCC_{1120-1212}$ (right). The phosphorylation of Ser1178 were further confirmed by the mass spectroscopy analysis (Figure S3).

(B) The same strategy was used to identify the third ERK2 phosphorylation site (Ser1267) of DCC using the $DCC_{1120-1326}$ fragment.

(C) No detectable phosphorylation of Ser1362 and Ser1390 by ERK2 could be observed.

(D) The phosphorylation of DCC by ERK2 requires the DCC docking sequence. The figure shows that deletion of the docking sequence ($DCC_{1120-1326}\Delta 1145-1154$) completely abolished its phosphorylation by ERK2 (see also Figure S3).

events is directly coupled with the MAPK signaling pathways (Yang et al., 2009). We further demonstrate that the conserved P1 domain of DCC mediates its interaction with ERK2. The crystal structure of the ERK2/DCC peptide complex reveals that the ERK2-binding P1 domain of DCC contains a typical docking sequence found in numerous MAPK substrates and MAPK regulatory enzymes. Most importantly, we discover that DCC is a direct substrate of ERK2. We show that the docking motif-mediated ERK2 binding is absolutely required for ERK2 phosphorylation of three residues (Ser1178, Thr1187, and Ser1267) in the cytoplasmic domain of DCC. This ERK2-mediated phosphorylation of DCC is likely to be physiologically relevant, as it has been shown that ERK2 can be activated by the netrin/DCC complex and that the activated ERK2 can be recruited to the DCC receptor complex (Campbell and Holt, 2003; Forcet et al., 2002). The direct phosphorylation of DCC by ERK2 immediately suggests that, in addition to being an adaptor serving to link the ERK1/2 signaling complexes, the cytoplasmic domain of DCC actively participates in signaling events in an ERK2 phosphorylation-dependent manner. One might envision that the ERK2-mediated phosphorylation of one or more of the three sites of DCC identified in this study may serve as regulatory switch(es) for DCC to interact with its downstream signaling partners (e.g., the SH2 domains of NCK, (Li et al., 2002)). Another possible function of ERK2-mediated phosphorylation of DCC could be disrupting the interactions of DCC with its binding partners, resulting in the downregulation of downstream signaling. How ERK1/2 activation and ERK1/2-mediated phosphorylation of DCC relate to DCC's direct downstream processes, however, remains to be established. Nonetheless, our findings strengthen the link between the ERK1/2 signaling pathway and netrin/DCC signaling events, and furthermore uncover a potentially new ERK1/2 phosphorylation-dependent DCC signaling mechanism. While this paper was in preparation, a report by Tcherkezian et al. (2010) was published, showing direct association of DCC with protein synthesis machinery for axon growth and development and the P1 domain is essential for this association. Interestingly, ERK2 was also identified to associate with DCC in their proteomic study. Since ERK2 activity is directly associated with protein synthesis via eIF2α (Monick et al., 2006) and eIF4E (Herbert et al., 2002), this report together with our study provides a strong link between ERK2 and DCC-mediated protein synthesis.

Docking motif-mediated binding is common in interactions between MAP kinases and their substrates or regulatory enzymes (Goldsmith et al., 2007). The ERK2/DCC interaction follows this common enzyme/substrate interaction mode. The P1 domain-mediated docking of DCC onto ERK2 increases the specificity and efficiency of the phosphorylation of DCC by the kinase, and deletion of the docking motif completely abolishes ERK2 phosphorylation of DCC even though the DCC cytoplasmic tail with P1 deletion retains a weak ERK2 binding capacity (Figure 2A). Our in vitro phosphorylation assay further showed that the three phosphorylation sites on DCC showed different phosphorylation efficiencies by ERK2 (in the decreasing order of Ser1178, Thr1187, and Ser1267; Figure 5). The differential phosphorylation efficiencies of the three sites by ERK2 can be nicely explained by the structure of the ERK2/DCC peptide complex. Ser1178 is closest to the C-terminal end of the docking motif and therefore is in the most favorable orientation to access the active site of ERK2. In contrast, Ser1267 is more than 110 residues away from the docking sequence of DCC (the entire

Table 1. Statistics of X-ray Crystallographic Data Collection and Model Refinement

Data collection	
Space group	P32
Unit cell parameters	
a, b, c (Å)	a = b = 87.309, c = 94.721
Resolution range (Å)	50.00–1.95 (1.98–1.95)
No. of unique reflections	30,642 (1538)
Redundancy	10.8 (10.6)
I/σ	36.28 (3.59)
Completeness (%)	99.9 (100.0)
R_{merge} (%)[a]	6.6 (67.0)
Structure refinement	
Resolution (Å)	47.23–1.95 (2.00–1.95)
R_{cryst}/R_{free} (%)[b]	19.9 (27.2)/24.0 (30.1)
rmsd bonds (Å)/angles (degree)	0.007/0.976
No. of reflections working set/test set	27547/1547
No. of atoms	
Protein atom	2845
Water molecules	176
Others	6
Average B factor of protein/peptide(Å^2)[c]	
Main chain	39.70/71.78
Side chain	42.57/79.03
Ramachandran plot	
Most favored regions	90.90%
Additionally allowed	8.70%
Generously allowed	0.30%

Numbers in parentheses represent the value for the highest resolution shell.

[a] $R_{merge} = \sum |I_i - I_m| / \sum I_i$, where I_i is the intensity of measured reflection and Im is the mean intensity of all symmetry related reflections.

[b] $R_{cryst} = \sum ||F_{obs}| - |F_{calc}|| / \sum |F_{obs}|$, where Fobs and Fcalc are observed and calculated structure factors. $R_{free} = \sum_T ||F_{obs}| - |F_{calc}|| / \sum_T |F_{obs}|$, where T is a test data set of about 5% of the total reflections randomly chosen and set aside prior to refinement.

[c] B factors are calculated by combining the residual B factor and TLS parameters using TLSANL program in CCP4.

cytoplasmic domain of DCC is essentially unstructured, our unpublished data) and therefore is in the least favorable position to be phosphorylated by ERK2. By the same logic, no phosphorylation could be detected for the two predicted ERK2 phosphorylation sites in the P2 (Thr1362) and the P2/P3-linker (Ser1390).

EXPERIMENTAL PROCEDURES

Protein Expression and Purification

The coding sequences of all DCC cytoplasmic constructs and mutants were PCR amplified from rat *DCC* and cloned into a PET-32a vector. The wild-type ERK2 and its mutants were cloned into PET-15b or PET-MBP.3C vectors for expressing different tagged ERK2. Proteins were expressed in BL21 *Escherichia coli* cells. The His_6-tagged proteins were purified using Ni^{2+}-NTA agarose column followed by size-exclusion chromatography. The GST fusion proteins were purified using GSH-Sepharose affinity chromatography. The constitutively active MEK1 (R4F, ΔN3/S218E/S222E) and N-terminal His_6-tagged ERK2 were co-expressed in BL21 (DE3) *E. coli* cells with the plasmid PET-His_6ERK2/R4F (a generous gift from Dr. Melanie Cobb, University of Texas Southwestern Medical Center, Dallas). The active ERK2 was expressed and purified following the strategy described previously (Heise and Cobb, 2006). The phosphorylation state of the purified, active ERK2 was verified by SDS-PAGE-based band shift and LC-ESI-MS/MS.

Affinity Purification with Rat Brain Lysate

Purified recombinant DCC fragments were individually coupled to CNBr-activated Sepharose beads following the manufacturer's instruction (GE, healthcare). In brief, DCC proteins were dialyzed into 0.1 M $NaHCO_3$ buffer (pH 8.3) containing 0.5 M NaCl. Activated beads and DCC proteins were mixed and shaken at room temperature for 1 hr. The remaining active groups on the beads were quenched by incubating with 0.1 M Tris at pH 8.0. The DCC coupled beads were first balanced with rat brain homogenate buffer (50 mM HEPES [pH 7.4] containing 0.1 M NaCl, 10% glycerol, 1 mM dithiothreitol, 1 mM EDTA, and the protease inhibitor cocktail from Roche) and then mixed with the rat brain homogenate at 4°C with shaking for 1 hr. After extensive washing, the bound proteins were eluted step-wisely with elution buffer containing 2 M, 4 M, 6 M Urea, and 1% SDS, respectively. The eluted proteins were precipitated with TCA. After drying, the precipitated proteins were resolved by an 18 cm 8%–15% gradient SDS-PAGE and detected using silver staining.

Mass Spectroscopy

Protein bands from the silver-stained gels were excised and digested with trypsin (Promega). The digested peptides were eluted with 0.1% TFA and 10% CAN and analyzed by a 4700 Proteomics Analysis mass spectrometer (Applied Biosystems). If necessary, the eluted peptide were separated by nanoLC and analyzed by an on-line LC-ESI-MS/MS. The MASCOT software was used to search the MALDI-TOF MS data. The LC- ESI-MS/MS data was analyzed using TurboSequest V. 27.

In Vitro Pull-Down Assay

Equal molar amount of GST and GST-fused DCC proteins (~3.7 nmol each) were loaded onto 20 μl of GSH-Sepharose 4B slurry beads (GE, HealthCare) in an assay buffer containing 50 mM Tris-HCl (pH 8.0), 100 mM NaCl, 1 mM EDTA, 1 mM DTT, and protease inhibitors. The protein loaded beads were then mixed with purified potential binders individually. After incubation for 3 hr at 4°C, and the beads were washed three times each with 500 μl of assay buffer. The proteins captured by GSH-Sepharose beads were eluted by boiling with the SDS-PAGE sample buffer and resolved and detected by 15% SDS-PAGE using Coomassie blue staining. In vitro MBP-tagged protein pull-down assay was carried out with the amylase magnetic beads (NEB) following the similar protocol as that described for the GSH-Sepharose pull-down experiment above.

Fluorescence Polarization Assay

Fluorescence polarization-based titration assays were performed on a PerkinElmer LS-55 fluorimeter equipped with an automated polarization at room temperature. Commercially synthesized DCC peptide was labeled with fluorescein-5-isothiocyanate (Invitrogen, Molecular Probe) at its N terminus. The labeled peptide was purified by passing through a Superdex Peptide 10/300GL column (GE, HealthCare) in the assay buffer (50 mM Tris-HCl [pH 8.0], 100 mM NaCl, 1 mM EDTA, and 1 mM DTT). The fluorescence polarization values of the FITC-labeled DCC peptide (~1 μM) were recorded with increasing amount of ERK2 or its mutants. The dissociation constant (K_d) was calculated by fitting the classical one binding site model.

Kinase Assay

About 1 mg/ml DCC fragments were dialyzed in the phosphorylation reaction buffer containing 20 mM Tris (pH 8.0), 10 mM $MgCl_2$, 100 mM NaCl, 2 mM DTT, and protease inhibitors at 30°C (Canagarajah et al., 1997; Yang et al., 2007). The concentration of active Erk2 and ATP were kept at 1 μg/ml and 0.1 mM, respectively. The reaction at each desired time point was stopped by boiling the assay mixtures with the SDS-PAGE sample buffer.

Crystallography

Crystal of ERK2 in complex with the DCC peptide was obtained by the hanging drop vapor diffusion method at 20°C. The DCC peptide (residues 1140–1166)

was commercially synthesized and purified by HPLC. Fresh purified ERK2 was concentrated to 9 mg/ml before saturating amount of the DCC peptide was added. The EER2/DCC complex crystals were obtained by mixing 1 μl of the complex with 1 μl buffer composed of 0.1 M HEPES (pH 6.9), 18% PEG3350, and 0.12 M KSCN.

The structure of the EER2/DCC complex was solve by the molecular replacement using the inactive ERK2 structure (PDB code 1ERK) as the search model with PHASER (Storoni et al., 2004). The initial model was rebuilt manually and then refined using REFMAC (Murshudov et al., 1997) against the 1.95 Å resolution data set. Further manual model building and adjustment were completed using COOT (Emsley and Cowtan, 2004). In the final stage, the TLS refinement was applied. TLS groups are determined by TLSMD server (http://skuld.bmsc.washington.edu/~tlsmd/index.html). The stereo-chemical quality of the final model was validated by PROCHECK (Laskowski et al., 1993). The final refinement statistics are listed in Table 1. The structure figures were prepared using the program PyMOL (http://pymol.sourceforge.net/).

ACCESSION NUMBERS

Coordinates for the ERK2-DCC peptide complex have been deposited in the Protein Data Bank (PDB accession number 3O71).

SUPPLEMENTAL INFORMATION

Supplemental Information includes three figures and can be found with this article online at doi:10.1016/j.str.2010.08.011.

ACKNOWLEDGMENTS

We thank Melanie Cobb (University of Texas Southwestern Medical Center, Dallas) for the active MEK1 and the full-length ERK2 constructs used in this study, Zhenguo Wu for critical comments, and Anthony Zhang for editing the manuscript. The X-ray diffraction data were collected at the beamline BL17U at Shanghai Synchrotron Radiation Facility of China. This work was supported by National High Technology Research Program of China (2006AA02A320), National Major Basic Research Program of China (2009CB918600), National Science Foundation of China (20973040), Shanghai Leading Academic Discipline Project (B108), and grants from the Research Grant Council of Hong Kong to M.Z. (HKUST663407, 663808, 664009, SEG_HKUST06, and CA07/08.SC01).

Received: May 26, 2010
Revised: July 31, 2010
Accepted: August 13, 2010
Published: November 9, 2010

REFERENCES

Akella, R., Moon, T.M., and Goldsmith, E.J. (2008). Unique MAP kinase binding sites. Biochim. Biophys. Acta *1784*, 48–55.

Arakawa, H. (2004). Netrin-1 and its receptors in tumorigenesis. Nat. Rev. Cancer *4*, 978–987.

Campbell, D.S., and Holt, C.E. (2003). Apoptotic pathway and MAPKs differentially regulate chemotropic responses of retinal growth cones. Neuron *37*, 939–952.

Canagarajah, B.J., Khokhlatchev, A., Cobb, M.H., and Goldsmith, E.J. (1997). Activation mechanism of the MAP kinase ERK2 by dual phosphorylation. Cell *90*, 859–869.

Carvalho, A.L., Chuang, A., Jiang, W.W., Lee, J., Begum, S., Poeta, L., Zhao, M., Jeronimo, C., Henrique, R., Nayak, C.S., et al. (2006). Deleted in colorectal cancer is a putative conditional tumor-suppressor gene inactivated by promoter hypermethylation in head and neck squamous cell carcinoma. Cancer Res. *66*, 9401–9407.

Chan, S.S., Zheng, H., Su, M.W., Wilk, R., Killeen, M.T., Hedgecock, E.M., and Culotti, J.G. (1996). UNC-40, a C. elegans homolog of DCC (deleted in colorectal cancer), is required in motile cells responding to UNC-6 netrin cues. Cell *87*, 187–195.

Chang, C.I., Xu, B.E., Akella, R., Cobb, M.H., and Goldsmith, E.J. (2002). Crystal structures of MAP kinase p38 complexed to the docking sites on its nuclear substrate MEF2A and activator MKK3b. Mol. Cell *9*, 1241–1249.

Downward, J. (2003). Targeting RAS signalling pathways in cancer therapy. Nat. Rev. Cancer *3*, 11–22.

Emsley, P., and Cowtan, K. (2004). Coot: model-building tools for molecular graphics. Acta Crystallogr. D Biol. Crystallogr. *60*, 2126–2132.

Fazeli, A., Dickinson, S.L., Hermiston, M.L., Tighe, R.V., Steen, R.G., Small, C.G., Stoeckli, E.T., Keino-Masu, K., Masu, M., Rayburn, H., et al. (1997). Phenotype of mice lacking functional deleted in colorectal cancer (Dcc) gene. Nature *386*, 796–804.

Fearon, E.R., Cho, K.R., Nigro, J.M., Kern, S.E., Simons, J.W., Ruppert, J.M., Hamilton, S.R., Preisinger, A.C., Thomas, G., Kinzler, K.W., et al. (1990). Identification of a chromosome 18q gene that is altered in colorectal cancers. Science *247*, 49–56.

Fitamant, J., Guenebeaud, C., Coissieux, M.-M., Guix, C., Treilleux, I., Scoazec, J.-Y., Bachelot, T., Bernet, A., and Mehlen, P. (2008). Netrin-1 expression confers a selective advantage for tumor cell survival in metastatic breast cancer. Proc. Natl. Acad. Sci. USA *105*, 4850–4855.

Forcet, C., Stein, E., Pays, L., Corset, V., Llambi, F., Tessier-Lavigne, M., and Mehlen, P. (2002). Netrin-1-mediated axon outgrowth requires deleted in colorectal cancer-dependent MAPK activation. Nature *417*, 443–447.

Goldschneider, D., and Mehlen, P. (2010). Dependence receptors: a new paradigm in cell signaling and cancer therapy. Oncogene *29*, 1865–1882.

Goldsmith, E.J., Cobb, M.H., and Chang, C.I. (2004). Structure of MAPKs. Methods Mol. Biol. *250*, 127–144.

Goldsmith, E.J., Akella, R., Min, X., Zhou, T., and Humphreys, J.M. (2007). Substrate and docking interactions in serine/threonine protein kinases. Chem. Rev. *107*, 5065–5081.

Heise, C.J., and Cobb, M.H. (2006). Expression and characterization of MAP kinases in bacteria. Methods *40*, 209–212.

Herbert, T.P., Tee, A.R., and Proud, C.G. (2002). The extracellular signal-regulated kinase pathway regulates the phosphorylation of 4E-BP1 at multiple sites. J. Biol. Chem. *277*, 11591–11596.

Hong, K., Hinck, L., Nishiyama, M., Poo, M.M., Tessier-Lavigne, M., and Stein, E. (1999). A ligand-gated association between cytoplasmic domains of UNC5 and DCC family receptors converts netrin-induced growth cone attraction to repulsion. Cell *97*, 927–941.

Hoshino, R., Chatani, Y., Yamori, T., Tsuruo, T., Oka, H., Yoshida, O., Shimada, Y., Ari-i, S., Wada, H., Fujimoto, J., and Kohno, M. (1999). Constitutive activation of the 41-/43-kDa mitogen-activated protein kinase signaling pathway in human tumors. Oncogene *18*, 813–822.

Keino-Masu, K., Masu, M., Hinck, L., Leonardo, E.D., Chan, S.S., Culotti, J.G., and Tessier-Lavigne, M. (1996). Deleted in colorectal cancer (DCC) encodes a netrin receptor. Cell *87*, 175–185.

Keleman, K., and Dickson, B.J. (2001). Short- and long-range repulsion by the Drosophila Unc5 netrin receptor. Neuron *32*, 605–617.

Kolodziej, P.A., Timpe, L.C., Mitchell, K.J., Fried, S.R., Goodman, C.S., Jan, L.Y., and Jan, Y.N. (1996). frazzled encodes a Drosophila member of the DCC immunoglobulin subfamily and is required for CNS and motor axon guidance. Cell *87*, 197–204.

Laskowski, R.A., Moss, D.S., and Thornton, J.M. (1993). Main-chain bond lengths and bond angles in protein structures. J. Mol. Biol. *231*, 1049–1067.

Leonardo, E.D., Hinck, L., Masu, M., Keino-Masu, K., Ackerman, S.L., and Tessier-Lavigne, M. (1997). Vertebrate homologues of C. elegans UNC-5 are candidate netrin receptors. Nature *386*, 833–838.

Li, X., Meriane, M., Triki, I., Shekarabi, M., Kennedy, T.E., Larose, L., and Lamarche-Vane, N. (2002). The adaptor protein Nck-1 couples the netrin-1 receptor DCC (deleted in colorectal cancer) to the activation of the small GTPase Rac1 through an atypical mechanism. J. Biol. Chem. *277*, 37788–37797.

Li, W., Lee, J., Vikis, H.G., Lee, S.H., Liu, G., Aurandt, J., Shen, T.L., Fearon, E.R., Guan, J.L., Han, M., et al. (2004). Activation of FAK and Src are receptor-proximal events required for netrin signaling. Nat. Neurosci. *7*, 1213–1221.

Li, X., Gao, X., Liu, G., Xiong, W., Wu, J., and Rao, Y. (2008). Netrin signal transduction and the guanine nucleotide exchange factor DOCK180 in attractive signaling. Nat. Neurosci. *11*, 28–35.

Liu, G., Beggs, H., Jurgensen, C., Park, H.T., Tang, H., Gorski, J., Jones, K.R., Reichardt, L.F., Wu, J., and Rao, Y. (2004). Netrin requires focal adhesion kinase and Src family kinases for axon outgrowth and attraction. Nat. Neurosci. *7*, 1222–1232.

Llambi, F., Causeret, F., Bloch-Gallego, E., and Mehlen, P. (2001). Netrin-1 acts as a survival factor via its receptors UNC5H and DCC. EMBO J. *20*, 2715–2722.

Mazelin, L., Bernet, A., Bonod-Bidaud, C., Pays, L., Arnaud, S., Gespach, C., Bredesen, D.E., Scoazec, J.Y., and Mehlen, P. (2004). Netrin-1 controls colorectal tumorigenesis by regulating apoptosis. Nature *431*, 80–84.

Monick, M.M., Powers, L.S., Gross, T.J., Flaherty, D.M., Barrett, C.W., and Hunninghake, G.W. (2006). Active ERK contributes to protein translation by preventing JNK-dependent inhibition of protein phosphatase 1. J. Immunol. *177*, 1636–1645.

Murshudov, G.N., Vagin, A.A., and Dodson, E.J. (1997). Refinement of macromolecular structures by the maximum-likelihood method. Acta Crystallogr. D Biol. Crystallogr. *53*, 240–255.

Park, H.H., Lo, Y.-C., Lin, S.-C., Wang, L., Yang, J.K., and Wu, H. (2007). The Death Domain Superfamily in Intracellular Signaling of Apoptosis and Inflammation. Annu. Rev. Immunol. *25*, 561–586.

Rajasekharan, S., Baker, K.A., Horn, K.E., Jarjour, A.A., Antel, J.P., and Kennedy, T.E. (2009). Netrin 1 and Dcc regulate oligodendrocyte process branching and membrane extension via Fyn and RhoA. Development *136*, 415–426.

Remenyi, A., Good, M.C., Bhattacharyya, R.P., and Lim, W.A. (2005). The role of docking interactions in mediating signaling input, output, and discrimination in the yeast MAPK network. Mol. Cell *20*, 951–962.

Ren, X.R., Ming, G.L., Xie, Y., Hong, Y., Sun, D.M., Zhao, Z.Q., Feng, Z., Wang, Q., Shim, S., Chen, Z.F., et al. (2004). Focal adhesion kinase in netrin-1 signaling. Nat. Neurosci. *7*, 1204–1212.

Storoni, L.C., McCoy, A.J., and Read, R.J. (2004). Likelihood-enhanced fast rotation functions. Acta Crystallogr. D Biol. Crystallogr. *60*, 432–438.

Tcherkezian, J., Brittis, P.A., Thomas, F., Roux, P.P., and Flanagan, J.G. (2010). Transmembrane receptor DCC associates with protein synthesis machinery and regulates translation. Cell *141*, 632–644.

Thiebault, K., Mazelin, L., Pays, L., Llambi, F., Joly, M.O., Scoazec, J.Y., Saurin, J.C., Romeo, G., and Mehlen, P. (2003). The netrin-1 receptors UNC5H are putative tumor suppressors controlling cell death commitment. Proc. Natl. Acad. Sci. USA *100*, 4173–4178.

Xie, Y., Ding, Y.Q., Hong, Y., Feng, Z., Navarre, S., Xi, C.X., Zhu, X.J., Wang, C.L., Ackerman, S.L., Kozlowski, D., et al. (2005). Phosphatidylinositol transfer protein-alpha in netrin-1-induced PLC signalling and neurite outgrowth. Nat. Cell Biol. *7*, 1124–1132.

Yang, Y., Zou, L., Wang, Y., Xu, K.S., Zhang, J.X., and Zhang, J.H. (2007). Axon guidance cue Netrin-1 has dual function in angiogenesis. Cancer Biol. Ther. *6*, 743–748.

Yang, L., Garbe, D.S., and Bashaw, G.J. (2009). A frazzled/DCC-dependent transcriptional switch regulates midline axon guidance. Science *324*, 944–947.

Zhang, F., Strand, A., Robbins, D., Cobb, M.H., and Goldsmith, E.J. (1994). Atomic structure of the MAP kinase ERK2 at 2.3 A resolution. Nature *367*, 704–711.

Zhou, T., Sun, L., Humphreys, J., and Goldsmith, E.J. (2006). Docking interactions induce exposure of activation loop in the MAP kinase ERK2. Structure *14*, 1011–1019.

Zhu, X.J., Wang, C.Z., Dai, P.G., Xie, Y., Song, N.N., Liu, Y., Du, Q.S., Mei, L., Ding, Y.Q., and Xiong, W.C. (2007). Myosin X regulates netrin receptors and functions in axonal path-finding. Nat. Cell Biol. *9*, 184–192.